*Transactions of the 17th International Conference on Structural Mechanics in Reactor Technology (*SMiRT 17)
Prague, Czech Republic, August 17 –22, 2003

Paper # H03-5

Shaking Table Test of RC Box-type Shear Wall in Multi-axes Loading

Yoshio Kitada[1)], Haruhiko Torita[2)], Ryoichiro Matsumoto[2)], Yoshinori Mihara[3)], Takao Nishikawa[4)]

[1)] Nuclear Power Engineering Corporation, Tokyo, Japan
[2)] Shimizu Corporation, Tokyo, Japan
[3)] Kajima Corporation, Tokyo, Japan
[4)] Tokyo Metropolitan University, Tokyo, Japan

ABSTRACT

Nuclear Power Engineering Corporation (NUPEC) is carrying out the test project, which is named 'Model Tests of Multi-Axes Loading on RC Shear Walls', focused on multi-axes loading of RC seismic shear walls. Dynamic tests using a shaking table of Public Works Research Institute in Japan were conducted, as a part of the test project.

A specimen consists of box-type shear walls, a base slab and an upper slab. Dimensions of the walls are 1.5 m square x 1m x 75 mm. Rebar arrangement for the walls is 2-D6@70 (pw=1.2%) in both vertical and horizontal direction. Normal concrete, design strength of which was about 35 MPa, was used for walls. Two specimens named DT-B-01 and DT-B-02 were tested to check the reproducibility of results.

Excitation was planned to determine the fundamental response properties of the specimens in wide range of responses from elastic one to ultimate one. Three components of input motion were made from uniform random numbers. The level of vertical acceleration in target response spectra is set half of those in horizontal directions. Six steps of excitation were set. Magnification of input acceleration were increased gradually step by step, from Run-1 for elastic response to Run-6 for ultimate response. Acceleration, displacement, strain of vertical wall reinforcement were measured and cracks were observed.

This paper outlines results of the dynamic tests. Also discussed are topics such as ratios of deformation components, applicability of skeleton curve of restoring force characteristics obtained in uni-axial loading, and equivalent viscous damping factor. A simple method to evaluate equivalent viscous damping factor is proposed, as shape of load-displacement relationship curves is tangled too much to apply usual method of evaluation.

KEY WORDS: RC seismic shear wall, multi-axes loading, model test, shaking table test, dynamic response

1. INTRODUCTION

Nuclear Power Engineering Corporation (NUPEC) is carrying out a test project focused on multi-axes loading of RC shear walls, which is named 'Model Tests of Multi-Axes Loading on RC Shear Walls' and is sponsored by Ministry of Economy, Trade and Industry of Japan (METI). Dynamic tests using a shaking table of Public Works Research Institute in Japan were conducted, as a part of the test project. Test program is described in the following section. Test results are outlined in section3. Some topics regarding response characteristics of specimens are also discussed.

2. OUTLINE OF TEST PROGRAM

2.1 Specimen

A specimen consists of box-type shear walls, a base slab and an upper slab. Dimensions of the walls are 1.5 m square x 1m x 75 mm. Rebar arrangement for the walls is 2-D6@70 (pw=1.2%) in both vertical and horizontal direction. Normal concrete with design strength of about 35 MPa was used for walls. Four blocks of weights, each of which weighed 15.62 ton, were attached on the upper slab with PC rods, to make axial stress at the bottom of walls due to dead load 1.47 MPa. Sum of weight of the four blocks, the upper slab and upper half of the walls was 71.45 ton. Two specimens named DT-B-01 and DT-B-02 are tested to check the reproducibility of test results. Shape, reinforcement, and material properties of the specimens are shown in Fig.1, Fig.2, and Table1 respectively.

2.2 Plan of Excitation and Measurement

Three components of artificial input motions, duration of which were 7 seconds, were made from uniform random numbers, so that sufficient test data, ranging from elastic ones to ultimate ones, to clarify dynamic response characteristics of the specimens can be obtained. The level of vertical acceleration in target response spectra is set half of those in horizontal directions. Six input steps of excitation shown in Fig.1 were set in the original excitation plan. These steps were executed from Run-1 to Run-6 with increasing input acceleration levels. Acceleration response spectra and acceleration time history of input motions are shown in Fig.4 and Fig.5.

Measurement plan was drawn up assuming that the upper slab and the base slab mostly behave like rigid bodies. Acceleration, displacement, strain of vertical wall reinforcement were measured. Arrangement of sensors for measuring displacement and acceleration are shown in Fig.6. Sampling period in data acquisition was 400Hz for DT-B-01 and Run-1&2 of DT-B-02, and 1000Hz for the rest. Low-pass filter, whose characteristics is shown in Fig.7, were used.

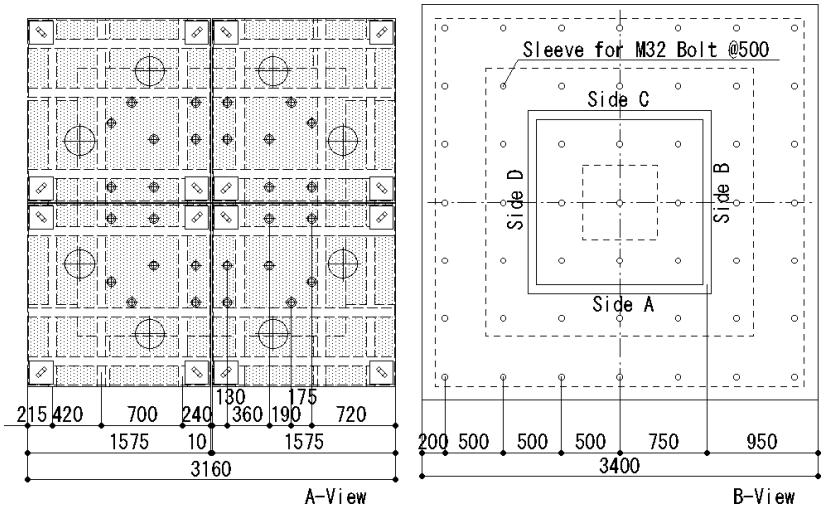

(a) Weight blocks (b) Walls and the base slab

Fig. 1 Shape of specimens (unit:mm)

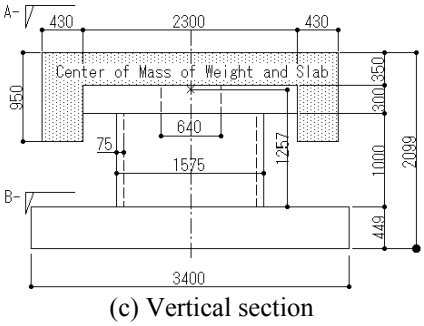

(c) Vertical section

Table1. Material properties

Mix proportion of concrete	DT-B-01	DT-B-02
Water cement ratio (%)	65.0	67.0
Sand aggregate ratio (%)	52.0	54.0
Unit water content (kg/m3)	178	180
Cement (kg/m3)	274	269
Sand (kg/m3)	951	969
Pea grabbel (kg/m3)	840	822
Pozolis#70 (kg/m3)	0.685	0.673

Concrete property	DT-B-01	DT-B-02
Comp. strength σ_B (MPa)	38.6	34.4
Comp. strain ε_0 at σ_B (μ)	-2033	-2207
Young's modulus E_c (GPa)	29.3	26.6
Poisson's ratio μ_c	0.20	0.19
Split tensile strength (MPa)	2.63	2.88
σ_B of upper slab (MPa)	46.8	40.5
σ_B of base slab (MPa)	39.7	43.6

Rebar(SD345, D6) property	DT-B-01	DT-B-02
Yield point fy (MPa)	381	378
Tensile strength fu (MPa)	499	501
Elongation (%)	29.1	29.8
Young's modulus Es (GPa)	171	185

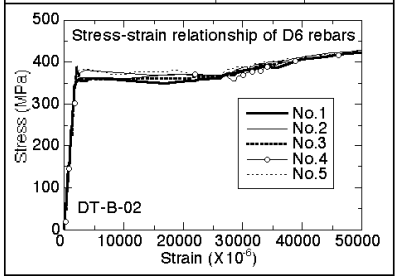

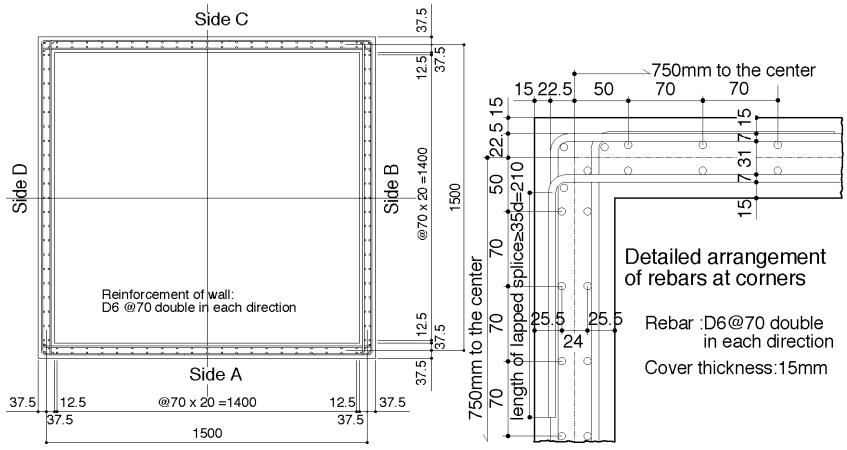

Fig.2 Rebar arrangement of walls

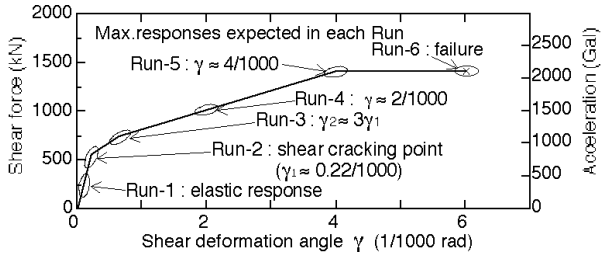

Fig.3 Maximum response expected in each Run

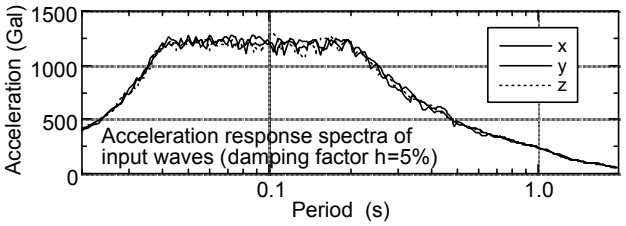

Fig.4 Acceleration response spectra of input waves

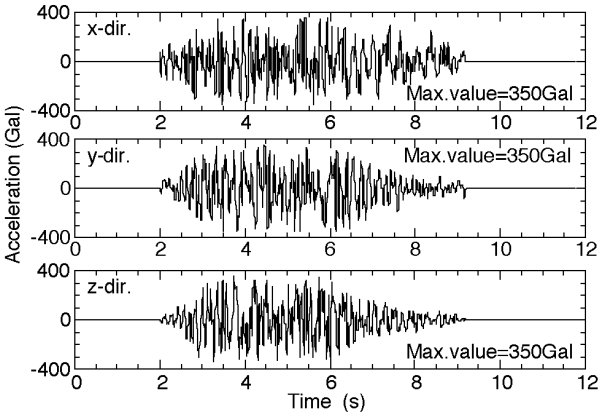

Fig.5 Time history of input acceleration waves

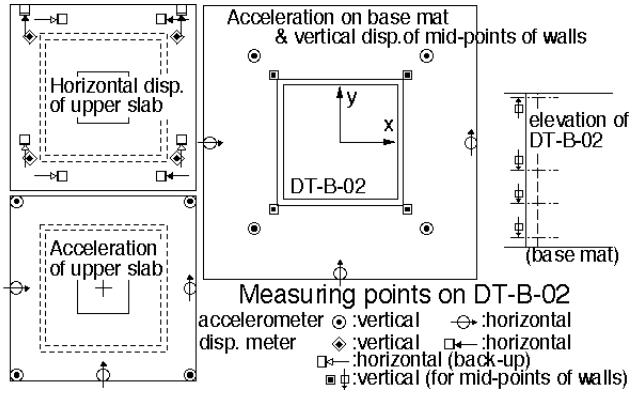

Fig.6 Measuring points on DT-B-02 specimen

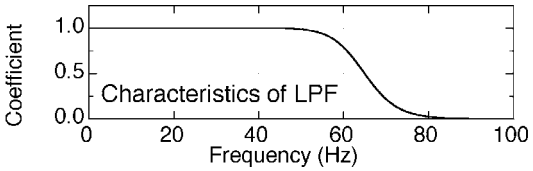

Fig.7 Characteristic of low-pass filter

3. THE TEST RESULT

3.1 Crack Patterns

Crack patterns observed in DT-B-02 are shown in Fig.8 as an example. Bending cracks were observed at the foot of the walls after Run-1. Initial shear cracks were found at the mid portion of the wall after the excitation step of Run-2, in which initiation of shear crack was expected. The number of cracks in the wall gradually increases after Run-2. In the final excitation step , concrete at the foot of the walls fell down totally.

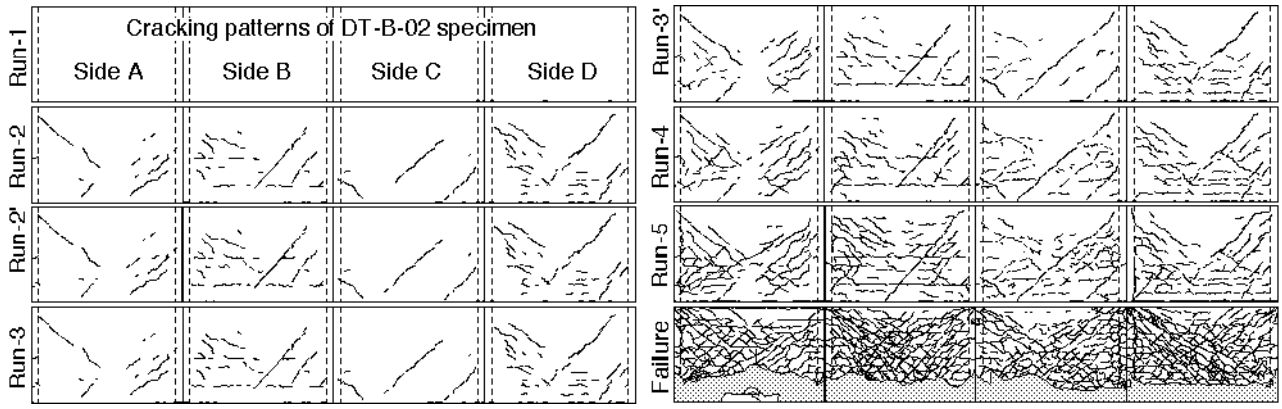

Fig.8 Cracking patterns of DT-B-02 specimen

3.2 Acceleration Time History and Hysteresis Curve of Response

Examples of the recorded horizontal acceleration time history of the upper slab and Hysteresis response curve regarding displacement and acceleration of DT-B-02 are shown in Figs. 9, 10 and 11.

Acceleration-displacement relationship curves of Fig.10 show that the slip nature of reverse-S shape in the graphs getting clearer as the excitation steps goes on. The second graph of Fig.11 shows a horizontal displacement-vertical displacement relationship curve. The curve shows shape like a shallow bowl. Residual vertical displacement shown in the graph means increase of bending cracks left unclosed.

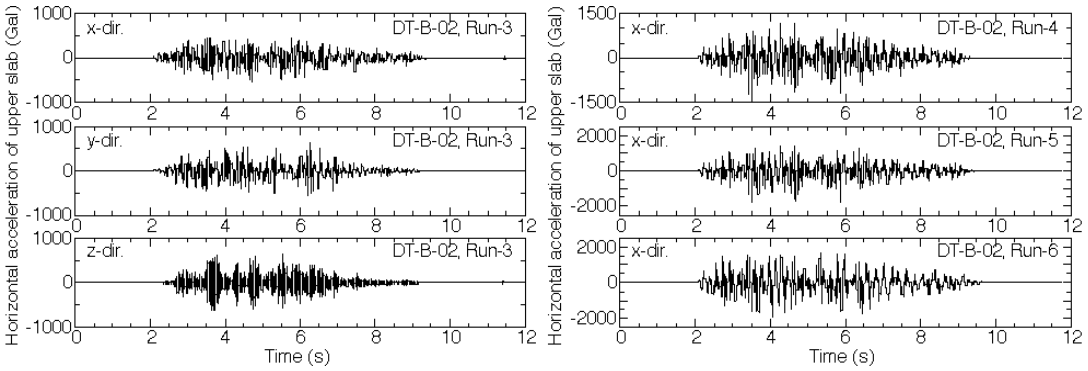

Fig.9 Time history of horizontal acceleration waves

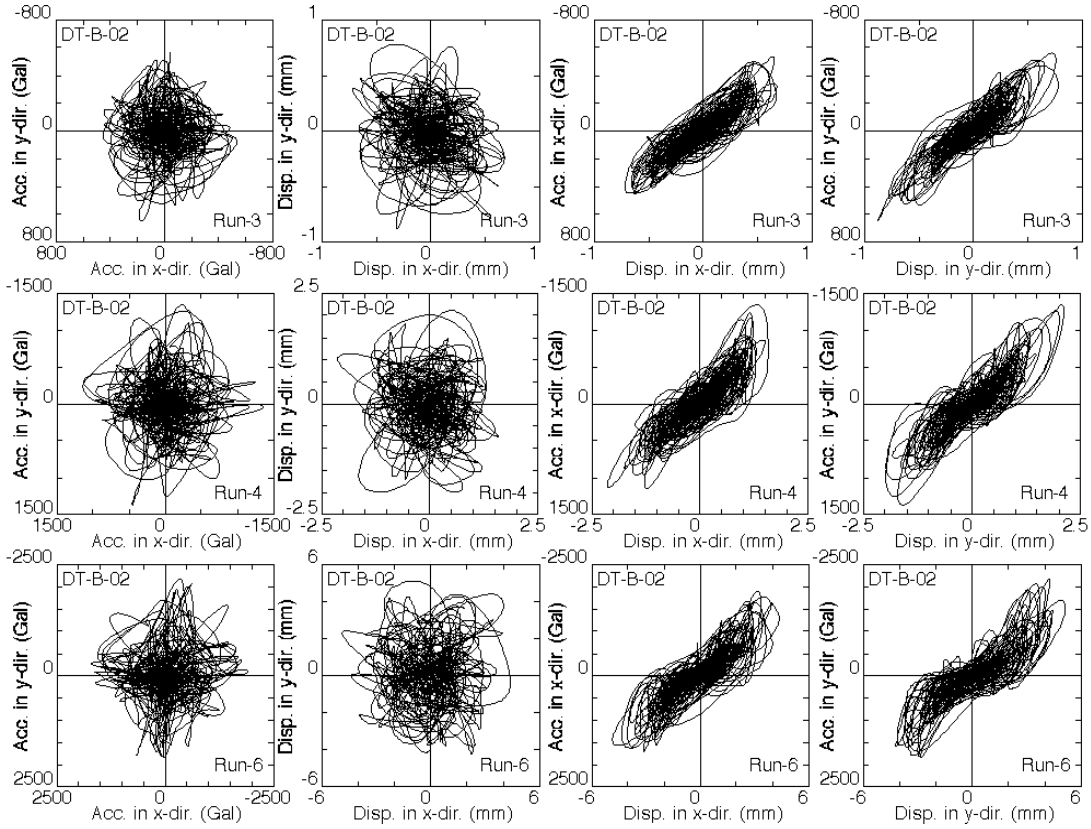

Fig.10 Hysteresis loop of horizontal response

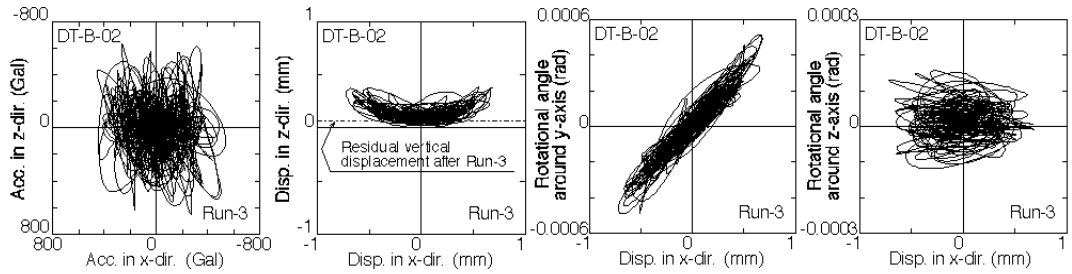

Fig.11 Hysteresis loop of horizontal response and other quantities

3.3 Changes of Responses

Table2 and Fig.12 show changes in natural frequencies. Maximum responses in each step are summarised in Table3.

Initial natural frequencies in horizontal directions were 22-23Hz in DT-B-01, and 20-21Hz in DT-B-02. These values fell down remarkably after experience of early steps of excitation to become 7-8Hz in DT-B-01 and 6-7Hz in DT-B-02 before failure.

If a target response level could not be attained, another excitation step was added. That is the reason why Run numbers of the tests differ from the original excitation plan shown in Fig.4.

Table2. Change of natural frequencies

DT-B-01	x-dir.	y-dir.	z-dir.	DT-B-02	x-dir.	y-dir.	z-dir.
Run-0	22.5	22.5	46.8	Run-1	20.6	20.4	42.8
Run-1	15.2	14.4	36.4	Run-2	20.3	22.3	44.5
Run-2	16.2	15.1	34.6	Run-2'	15.4	13.8	39.2
Run-3	13.1	14.2	33.4	Run-3	15.2	13.6	39.6
Run-3'	11.5	13.1	33.0	Run-3'	14.8	13.4	39.5
Run-4	12.0	12.5	30.6	Run-4	14.5	13.0	39.5
Run-5	12.5	11.8	33.8	Run-5	14.3	12.2	38.1
Run-6	8.8	7.2	29.9	Run-6	13.0	11.5	37.9
f_1 before each Run (Hz)				Run-7	7.3	6.4	32.4

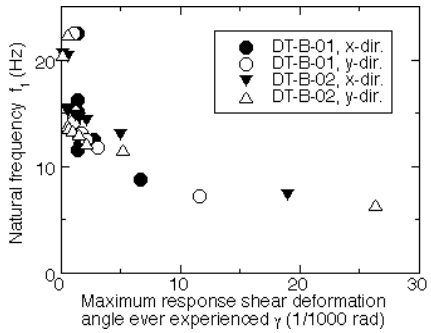

Fig.12 Relationship between γ and f_1

Table3. Maximum responses in each excitation step

DT-B-01	Run-0	Run-1	Run-2	Run-3	Run-3'	Run-4	Run-5	Run-6
αxbase [Gal]	-1512	-165	384	460	-735	-1162	-1617	-1678
αybase [Gal]	-499	-151	-518	761	-906	-1171	-1554	-1726
αzbase [Gal]	1537	-105	321	515	721	996	-985	635
βxbase [rad/s²]	-2.32	-0.55	1.82	2.29	-2.72	2.50	2.80	-1.89
βybase [rad/s²]	-10.76	-0.67	-2.18	2.46	-4.29	-5.84	7.14	-7.65
βzbase [rad/s²]	2.10	0.08	-0.25	-0.35	0.55	0.59	1.03	0.91
αxtop [Gal]	-1094	287	-549	-720	-1018	-1465	-1941	1752
αytop [Gal]	-564	-237	-629	1072	1700	1797	2307	-2448
αztop [Gal]	-2498	250	-669	969	1350	1726	1905	1490
βxtop [rad/s²]	-7.37	-1.82	8.86	10.41	14.30	14.53	16.77	-17.63
βytop [rad/s²]	-19.54	2.15	5.25	-6.55	-9.82	12.19	-16.04	13.98
βztop [rad/s²]	5.56	0.44	1.48	-1.93	-3.01	3.27	5.08	4.02
Ux [mm]	1.520	0.351	0.767	1.209	1.863	2.704	4.288	8.806
Uy [mm]	-0.443	-0.259	0.858	-1.383	-2.499	-2.765	-4.246	15.215
Uz [mm]	1.048	0.240	0.420	0.724	4.121	1.248	1.894	3.715
-θx [0.001 rad]	-0.435	0.122	0.749	0.929	3.502	1.540	1.964	4.131
θy [0.001 rad]	-1.544	0.225	0.488	0.677	-4.070	1.759	2.644	-2.140
θz [0.001 rad]	-0.071	-0.056	-0.171	0.327	-0.554	0.804	-1.156	4.262
γx [0.001 rad]	1.345	-0.218	0.472	0.712	-1.097	1.620	2.699	6.635
γy [0.001 rad]	1.065	-0.180	-0.501	-0.845	-1.651	-2.067	-3.104	11.559
Ubx [mm]	0.671	0.084	0.188	0.272	0.499	0.682	-0.644	-0.652
Uby [mm]	-0.743	0.059	0.289	0.367	0.555	-0.802	0.712	-0.542
Qx [kN]	733	-192	368	482	682	981	1300	-1173
Qy [kN]	378	159	422	-718	-1139	-1204	-1545	1639
Nz [kN]	2213	825	1052	1306	1561	1813	1933	1655
Tz [kN m]	-622	-49	-166	216	338	-366	-570	-451

DT-B-02	Run-1	Run-2	Run-2'	Run-3	Run-3'	Run-4	Run-5	Run-6	Run-7
αxbase [Gal]	143	933	256	484	1063	1005	1499	-1950	-1551
αybase [Gal]	-122	-836	-171	341	-740	973	-1198	-2096	-1886
αzbase [Gal]	85	839	181	375	777	712	1050	1385	941
βxbase [rad/s²]	-0.39	-2.29	-0.46	1.07	2.18	2.66	3.46	4.05	-2.42
βybase [rad/s²]	-0.50	3.25	-0.76	1.44	-4.22	3.69	6.47	8.04	1.87
βzbase [rad/s²]	-0.10	0.53	0.18	-0.22	0.52	0.57	0.77	-1.17	-0.79
αxtop [Gal]	-456	-853	-358	-535	-1187	-1356	-1780	-1902	-2101
αytop [Gal]	376	-712	338	650	-1077	1376	1709	-2164	-2966
αztop [Gal]	-182	1152	285	650	-1786	-1395	2104	2190	1435
βxtop [rad/s²]	-2.99	-7.97	-1.70	4.22	8.62	-11.75	12.71	18.78	16.80
βytop [rad/s²]	3.45	9.66	3.68	-5.64	-12.13	-12.15	-15.19	17.03	-14.76
βztop [rad/s²]	-0.30	1.79	0.55	1.50	-2.80	-2.63	4.07	-4.65	5.54
Ux [mm]	0.249	-0.953	-0.470	-0.721	-1.761	-2.132	-2.991	-4.901	18.941
Uy [mm]	-0.216	-1.004	-0.451	-0.878	1.437	2.113	3.028	5.135	-26.349
Uz [mm]	0.018	0.620	0.200	0.385	0.814	0.925	1.297	–	–
-θx [0.001 rad]	-0.109	-0.673	0.179	0.471	0.843	-1.036	-1.272	–	–
θy [0.001 rad]	-0.138	-0.909	-0.280	0.516	-1.087	1.126	1.805	–	–
θz [0.001 rad]	0.030	0.189	0.081	0.156	0.386	-0.518	0.609	1.548	10.786
γx [0.001 rad]	0.145	-0.530	-0.312	-0.436	-1.138	-1.454	-2.101	-4.901	18.941
γy [0.001 rad]	-0.138	-0.573	-0.342	-0.588	0.993	1.491	2.143	5.135	-26.349
Ubx [mm]	-0.028	-0.430	-0.177	-0.297	-0.536	-0.554	-0.763	–	–
Uby [mm]	-0.022	0.294	-0.104	-0.200	-0.367	-0.481	-0.631	–	–
Qx [kN]	306	571	240	358	795	908	1192	1274	1408
Qy [kN]	-252	477	-227	-435	721	-922	-1145	1450	1987
Nz [kN]	757	1429	848	1092	1836	1588	2067	2125	1619
Tz [kN m]	34	-200	-62	-168	314	295	-456	521	-621

(Note) α,β :sway and rotational acceleration, u,θ :sway and rotational displacement, γ :shear deformation angle, u_b :flexural component of horizontal displacement
Q,N,T :shear force, axial force, and torque around vertical axis, base,top :suffix to distinguish the base slab and the upper slab
Max. values before failure are adopted for the last Runs.

3.4 Deformation Component Ratios

Horizontal displacement of the upper slab contains not only flexural and shear deformation of the walls, but also displacement caused by rotation. As flexural cracks form and open at boundaries between the walls and the slabs, the walls and the upper slab rotate. Though D6 is the smallest size deformed bar available, bar diameter is relatively big compared to the size of the walls. It is also true that ribs on the surface of the bar is quite small compared to aggregate

size. So it is expected that vertical reinforcing bars of the walls tend to pull out from the slabs and that rotation at the foot of the walls is pretty big.

Rotations at z=0-60mm and z=970-1000mm, where z is a height from the surface of the base slab, are calculated from data of vertical displacement meters. Flexural deflection curve of the walls can be estimated from rotations at z=60,280,500 and 970mm, as is shown in Fig.13.

Thus horizontal displacement can be decomposed into four components; flexural deformation, shear deformation, deformation at top part of the walls, and deformation at the bottom part of the walls including displacement due to rotation. Ratios of four components to the total displacement at every moment are averaged in the manner shown in Fig.14. Transition of the ratios as excitation steps go on are shown in Fig.15.

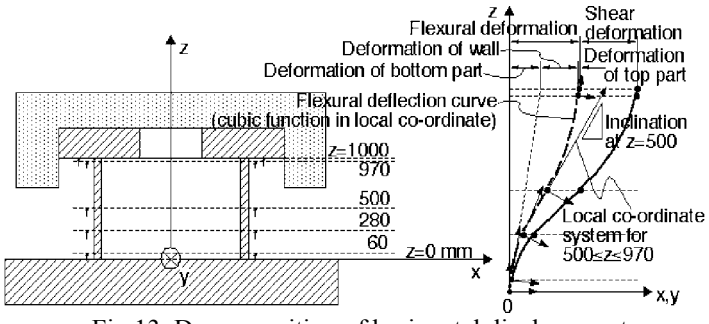

Fig.13 Decomposition of horizontal displacement

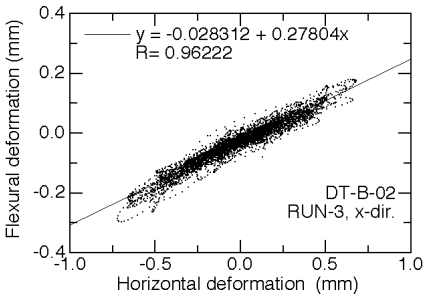

Fig.14 Linear regression to determine the ratio of flexural component to the total deformation

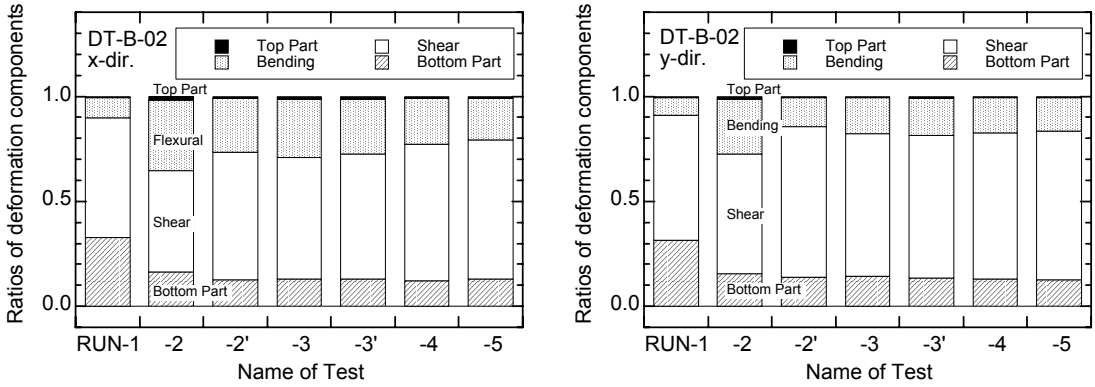

Fig.15 Transition of ratios of deformation components relative to the total deformation

3.5 Comparison of Maximum Response Values and Skeleton Curves for Uni-axial Loading

Some points of response of DT-B-02 specimen, where the record of maximum response acceleration in a horizontal direction were renewed, are plotted in Fig.16. Horizontal deformation angle means horizontal displacement divided by the height of the walls. Also plotted are examples of skeleton curves for uni-axial loading evaluated by equations adopted in JEAG 4601 [1,2], which is a technical guidelines for seismic design of nuclear power plant in Japan. A ratio between shear deformation and flexural one is assumed to be 6:4 and 8:2 according to Fig.15. Fluctuation band of vertical response acceleration is taken as ±1G.

Comparing test results to evaluated curves for uni-axial loading, the latter can be used as the first order approximation to the former, if used in the region where nonlinearity is weak. The differences between them at R≥2/1000, however, are not so small and more studies and discussions are necessary.

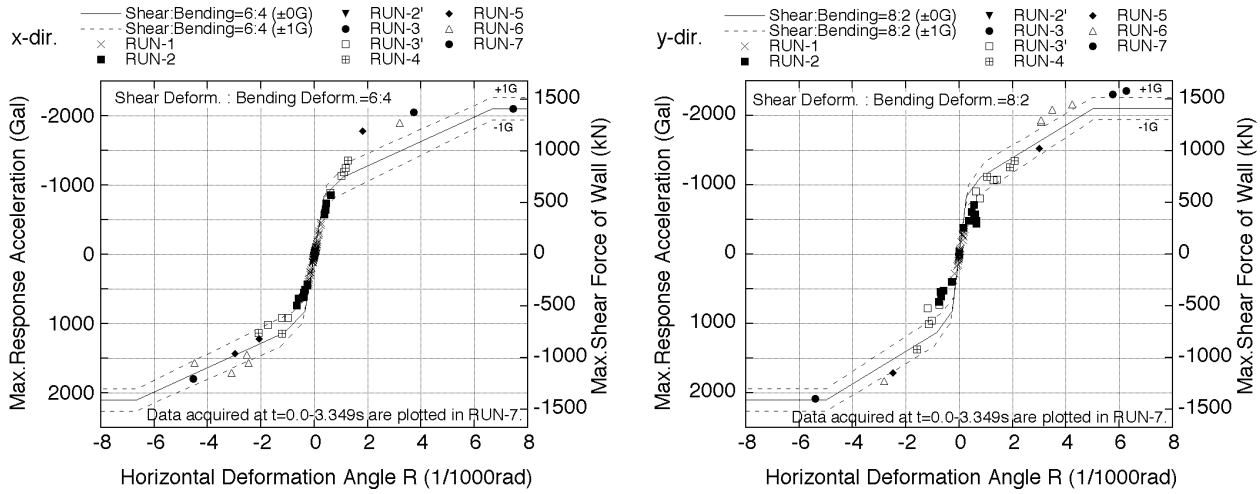

Fig.16 Renewal points of maximum response acceleration record compared with evaluated skeleton curves for uni-axial loading

3.6 Evaluation of Equivalent Viscous Damping Factor

Equivalent viscous damping factor heq is derived ordinarily from a hysrteresis loop of load-deformation relationship in the manner described in the left of Fig.17(a). In case of multi-axial loading, shape of load-deformation curves is tangled too much to apply usual method. It is also true that the time to draw a loop in x-direction seldom coincides with the time to draw a loop in y-direction. So a simple method shown in Fig.17(a) is used for trial estimation of heq.

At first, a linear system is determined applying linear regression analysis to load-deformation relationship data like Fig.18. In this equivalent linear system, small increment of elastic strain energy between i-th and i+1-th data is defined as ΔEi . The test data shows some deviation from the linear system in a sense of energy. A small increment of the deviation is defined as ΔWi. It is easy to calculate ΔEi and ΔWi at every moment. Equivalent viscous damping factor can be derived from sum of sufficient numbers of these increments using equation in Fig.17(a).

The left graph of Fig.19 shows heq calculated by cummulation of ΔWi and ΔEi from the beginning of excitation. Damping factor heq tends to some value as number of data increases. The right half of Fig.19 shows transition of heq derived by 1sec-running mean. The reason why heq decreases after t=5.5sec seems to be in the envelope shape of the input excitation. Fig.20 and Fig.21 are heq by running mean calculated in period1 and period2 shown in Fig.17(b). X-axis is the maximum value of deformation angle among all data within a width of running mean. It seems that values of heq in the left graphs regarding period1 are about 0.02 higher than those in the right graphs regarding period2 because of plastic hysteresis damping due to strong excitation.

As a trial, the same procedure as is written above is applied to the test results of uni-axial loading[3,4]. Accerelation time history of input motion for the specimen U-1 is shown in Fig.22(a). Duration time of input excitation in this test is not so long, and amplitude of acceleration is large in period4 shown in Fig.22(a). So in Run-3 and Run-4 of U-1, data in period4 are processed. In case of Run-5 of U-1, however, data in period3 are used because of the failure of the specimen. Fig.22(b) shows that heq of Run-5 of U-1 just before failure fairly coinsides with heq of DT-B-02 in period2, which includes plastic hysteresis damping. As heq of Run-3 and Run-4 of U-1 is close to heq of DT-B-02 in period1, it seems that plastic deformation is not so dominant in these Run.

The equivalent viscous damping factor derived in period1 can be taken as the lower limit of the factor of total damping including plastic hysteresis damping. On the other hand, the heq value derived in period2 shows the upper limit of sum of factors of viscous damping and structural damping, becauise it may include small plastic hysteresis damping. It is necessary to study more test results to determine an appropriate value of damping factor for multi-axial loading case.

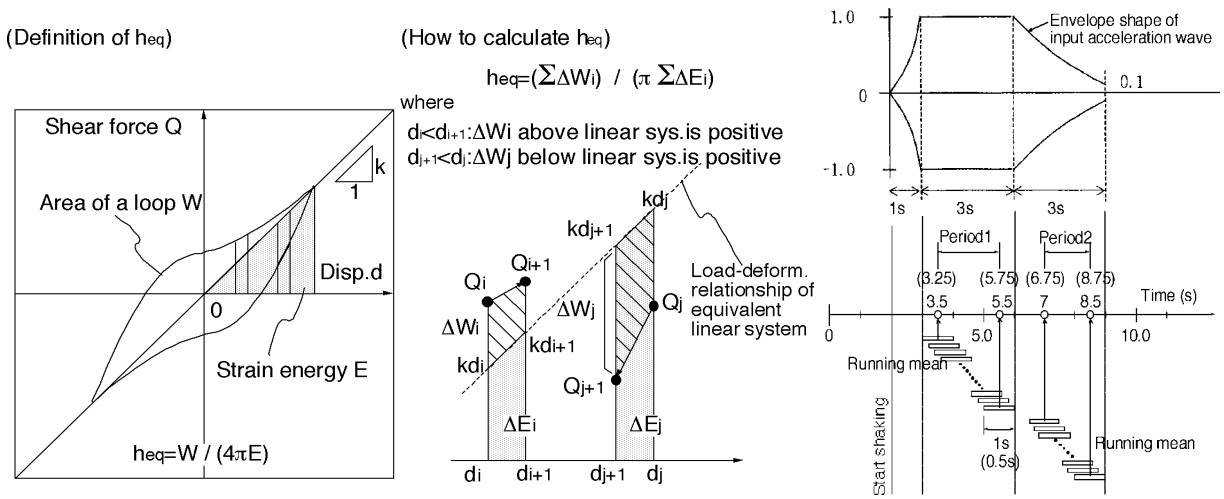

(a) Method of calculating heq (b) Data sampling periods for Fig.20&21

Fig.17 Method to evaluate equivalent viscous damping factor

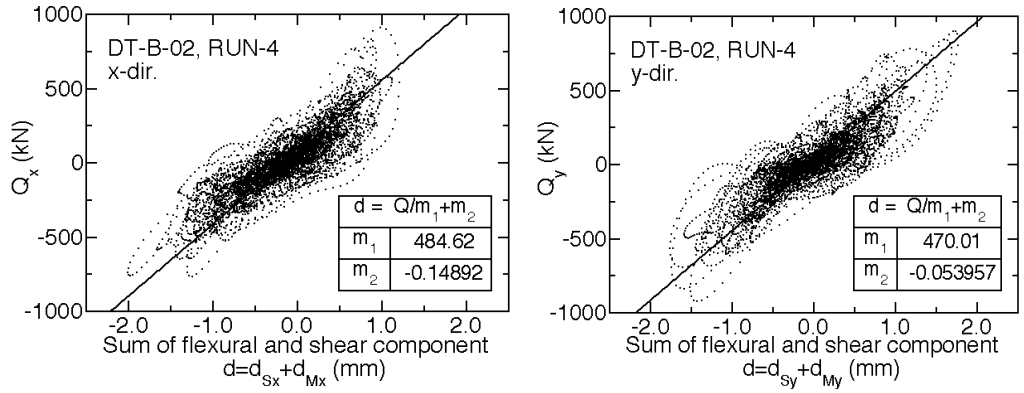

Fig.18 Linear regression to determine equivalent linear system

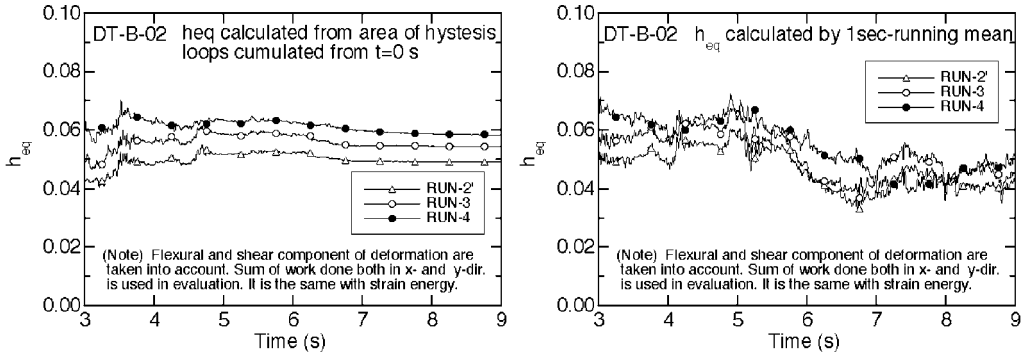

Fig.19 Transition of equivalent viscous damping factor

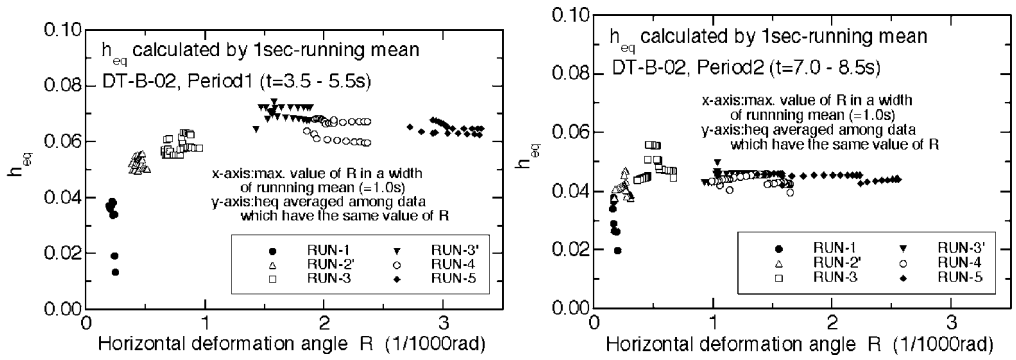

Fig.20 heq calculated by 1sec-running mean and related to max. deformation angle

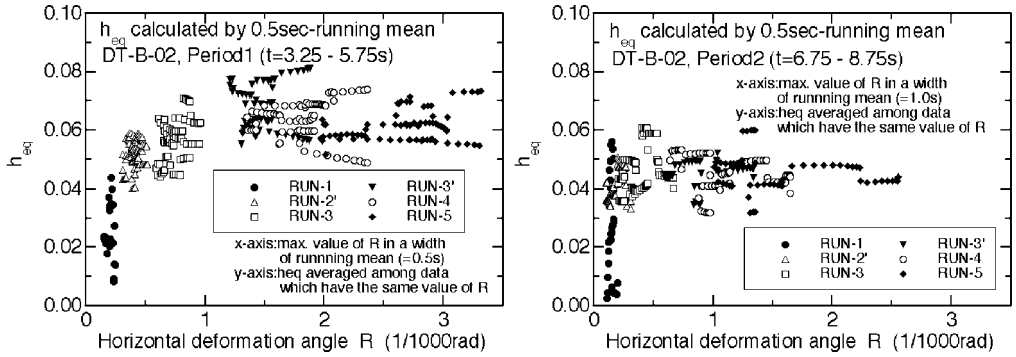

Fig.21 heq calculated by 0.5sec-running mean and related to max. deformation angle

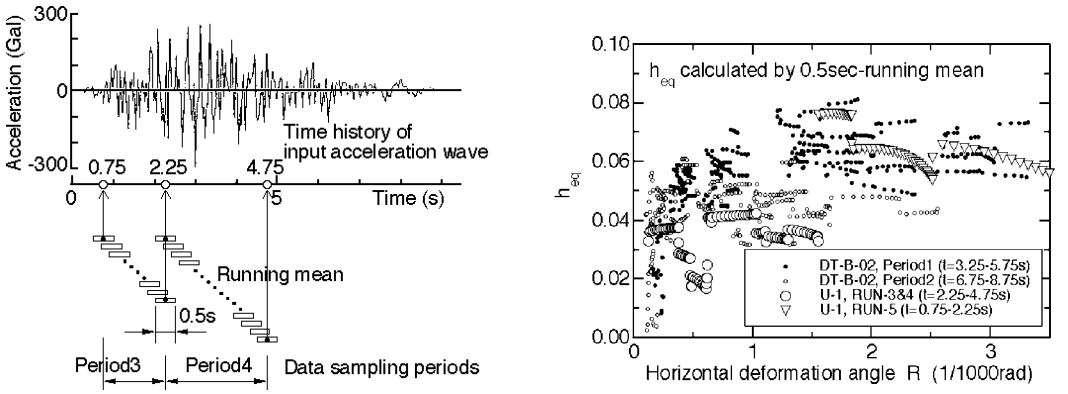

(a) Input motion and data sampling periods (b) Comparison with results of DT-B-02

Fig.22 Equivalent viscous damping factor of uni-axial dynamic loading test[3,4]

4. CONCLUDING REMARKS

Two box style RC shear wall specimens subjected to multi-directional input motions were tested and test data of specimens were obtained, to study fundamental response properties of RC seismic shear walls in wide range of responses from elastic one to ultimate one. Some characteristics of RC seismic shear walls were discussed. The reproducibility of the test results was checked.

The results will be used to improve seismic safety analysis codes relevant to multi directional inputs and will contribute to improve the method of evaluating safety of NPP buildings.

ACKNOWLEDGEMENTS

This work was performed by NUPEC as a part of the "Model Test of Multi-axis Loading on RC Shear Walls" project commissioned by the Ministry of Economy, Trade and Industry (METI) of Japan. Technical issues have been

discussed in the advisory committee on the project established by NUPEC (Chairperson: Professor Dr. Nishikawa). The authors wish to express their thanks to all the members of the committee for their valuable suggestions and co-operation.

REFERENCES

1. Survey Committee for Electrotechnical Standard, Japan Electric Association, "*Technical Guidelines for Aseismic Design of Nuclear Power Plants*" *(In Japanese)*, JEAG 4601-1987,1991, Japan Electric Association, Tokyo, JAPAN, 1987,1991.
2. Park,Y.J. and Hofmayer,C.H., "*Technical Guidelines for Aseismic Design of Nuclear Power Plants, Translation of JEAG 4601-1987*", NUREG/CR-6241, BNL-NUREG-52422, Brookheaven National Laboratory, Upton, N.Y., U.S.A., June 1994.
3. OECD/NEA/CSNI, "*SEISMIC SHEAR WALL ISP, NUPEC'S SEISMIC ULTIMATE DYNAMIC RESPONSE TEST, -Comparison Report-*", NEA/CSNI/R(96)10, OECD/GD(96)188, 1996.
4. Kitada,Y., Akino,K., Terada,K., Aoyama,H. and Miller,A., "Report on seismic shear wall international standard problem organized by OECD/NEA/CSNI", *Transactions of the 14th SMiRT*, Vol5, pp.321-332.